ITK-based Registration of Large Images from Light Microscopy: A Biomedical Application

K. Mosaliganti[1], T. Pan[2], R. Machiraju[1], K. Huang[2], and J. Saltz[2]

Department of [1]Computer Science and Engineering, [2]Biomedical Informatics
The Ohio State University, Columbus, Ohio, USA
kishore@bmi.osu.edu

Abstract. Inactivation of the retinoblastoma gene in mouse embryos results in morphological changes in the placenta, which has been shown to affect fetal survivability. The construction of a 3D virtual placenta aids in accurately quantifying structural changes using image analysis. The placenta dataset consisted of 786 images totaling 550 GB in size, which were registered into a volumetric dataset using ITK's registration framework. The registration process faces many challenges arising from the large image sizes, damages during sectioning, staining gradients both within and across sections, and background noise leading to local solutions. In this work, we implement a rigorous ITK-based preprocessing pipeline for removing noise and employ a novel 2-level optimization strategy for enhanced registration in ITK. We provide 3D visualizations and numerical results to demonstrate our improvements.

1 Introduction

Many human diseases have genetic bases that manifest phenotypically as functional and/or structural deficiencies. The retinoblastoma (Rb) gene is one of the first to be associated with a specific cancer, and has been studied extensively in both human cells and mouse models [1]. Recently, it has been shown that inactivation of Rb (Rb^{-}) in mouse embryo results in morphological changes in the placenta, including reduction in vascularity of the labyrinth layer. Figure 1 shows a sample slide with the approximate *labyrinth*, *spongiotrophoblast* and *glycogen* layers. The labyrinth layer serves the critical function of gas, nutrient, and waste exchange between the mother and the fetus and hence understanding its interaction with neighboring tissue layers is important. A decrease in vascularity is thought to contributes to fetal death at 14.5 days of gestation [2].

Image analysis of the structural changes in mouse placenta provides an opportunity for quantitative correlation of genetic changes with phenotype expressions. Specifically, the goals of image analysis are segmentation of the tissue layers, visualization of the finger-like infiltrations into the labyrinth, and quantitative measurement of volume and surface area of the layers. Registration of the tissue sections is therefore, an important pre-processing step for various algorithms as shown in Fig. 1 (Right), and its accuracy directly affects the quantification and

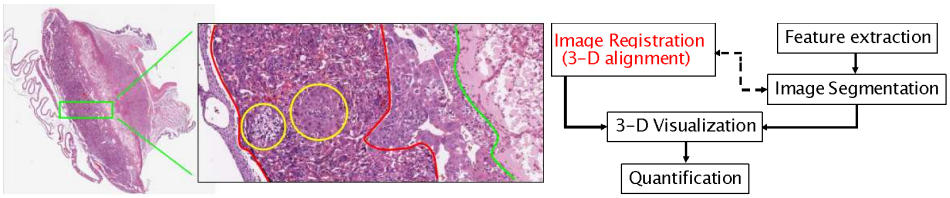

Fig. 1. Left: Placenta slice showing different tissue types. A small region magnified to show labyrinth layer (within red boundaries), spongiotrophoblast layer (between the red and green boundaries) and spongiotrophoblast and glycogen infiltrations (yellow circles). Right: Overall image analysis framework

interpretation of the results. Mutant (Rb^{-}) placenta was harvested at 13.5 days of gestation and prepared using a standard histological protocol. It was fixed in paraffin and sectioned at $3\mu m$ thickness using a microtome. Serial sections were mounted on glass slides and stained with hematoxylin and eosin. The slides are scanned in an Aperio ScanScope slide digitizer at *200x* magnification. The image dimensions on average were (15K x 15K x 3). The entire placenta produced *786* color images, ranging in size from *500 MB* to *1 GB* each. The manual nature of the tissue preparation process required extensive preprocessing steps as well as modifications to the registration process. Our pipeline was implemented in in the National Library of Medicine's (NIH/NLM) Insight Segmentation and Registration Toolkit (ITK) [3]. The following artifacts were observed in the images:

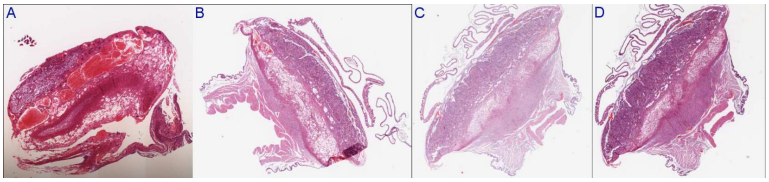

Fig. 2. A: background noise from acquisition. B: tissue tear and shear. C,D: consecutive sections have non-linear intensity variations.

1. Orientation differences: Sections are mounted in different orientations on glass slides due to the manual nature of the process.
2. Luminance gradient: Sections mounted close to the edge of the glass slide produce images with significant luminance gradients (Fig. 2A).
3. Non-tissue noise: Dust and air bubbles in the slide may cause artifacts.
4. Damaged and missing sections: During sectioning and mounting, sections are occasionally torn, folded, or discarded entirely. (Fig. 2B).
5. Staining variations: Differences in section thickness, staining duration, and

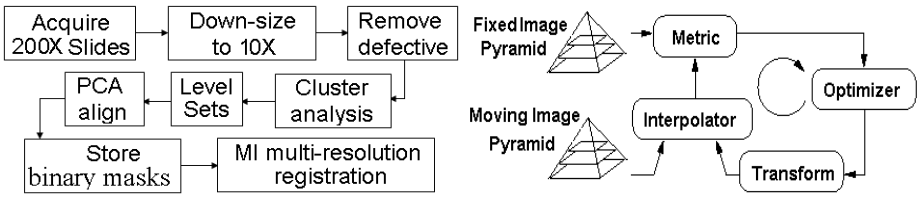

Fig. 3. Left: Pre-processing pipeline. Right: ITK-based registration framework. Transforms are scaled when passed from a lower to higher resolution.

stain concentration result in color variations (Fig. 2C,D).

In what follows, Section 2 explains the ITK framework for noise removal with the details of our registration framework components in Section 3. Section 4 provides details on our new optimization strategy with experimental and visualization results. Finally, we report our conclusions and outline our plans for the future in Section 5.

2 Preprocessing Framework

Defective Section Exclusion: Defective sections are identified using manual inspection and excluded from the pipeline. They are later accounted for in the 3D reconstruction and visualization process.
Tissue Detection: The first step separates the tissue (foreground) from the background (noise). We use the k-BCC clustering approach [4] with multi-resolution kd-tree optimizations for tissue detection, as it performs well in the presence of luminance gradient, background noise, and staining variations. It is a variation of the popular k-means algorithm adapted to the light microscopy images. It is validated for the placenta slices and compared with the Expectation Maximization (EM) and k-means clustering in [4]. Tissue pixels are identified and stored as binary masks which are used in the level-set based edge detection and the PCA alignment of sections.
Level-Sets for edge detection The binary mask obtained from the clustering algorithm has a poor description of the placenta boundary as shown in Figure 4. Moreover, parts of the placenta interior that were initially occupied by tissues of low luminance (such as vasculature) are clustered as background. These hollow regions also contribute to noise when evaluating the registration match across images since they are usually not well-correlated. Therefore, by using level-sets [5], an accurate boundary description is obtained by growing a contour inwards from the edges of the image boundary.
PCA Alignment: The possible translations and rotations in a plane define the transform space for the placenta images. Using *a priori* knowledge that mouse placenta sections are typically elongated in shape, we use principle component analysis (PCA) to estimate tissue orientation. The orientations are used to initialize registration, thus restricting the transform search space. PCA is performed

Fig. 4. Left: An example binary mask obtained from the KBCC algorithm. Center:An example tissue mask image from level-sets. Right: Top sequence shows the initial random orientation of the placenta images. The bottom sequence shows PCA-aligned images.

for each tissue mask image. The gleaned orientation angle is used to rotate and align the original histology images. Figure 4 shows the same two sequences of images before and after PCA alignment.

3 Mutual Information Based Registration

While the placenta images are acquired using the same staining protocol, they have multimodal characteristics due to non-linear variations in pixel intensities. This may be attributed to different stain absorptions, tissue thickness and luminance gradients. Under these conditions, it is difficult to detect appropriate landmarks for point or surface-based registration [6]. Intramodal registration methods that rely on linear correlation of pixel values are also inadequate [7]. Mutual information (MI) [8] based methods are effective in registering multimodal images with non-linear pixel intensity correlations.

We perform registration as an optimization process that searches for an image transform that allows the closest similarity between consecutive images. The input is a pair of stationary (S) and moving (M) images. The framework iteratively passes M through 4 stages: *transform*, *metric*, *optimizer*, and *interpolator* as shown in Figure 3 (Right). At a given iteration, the *transform* stage applies transform T_n on M which is then resampled onto a grid in the *interpolator* stage to yield $T_n(M)$. The *metric* stage computes the goodness of fit between S and $T_n(M)$. Based on the similarity metric values from current and prior iterations, the optimizer produces a refinement in transform T_{n+1}. At convergence, S and $T_n(M)$ have the optimal metric value thereby aligning the images. For the placenta dataset, we register each image to its predecessor, and the pairwise transforms were merged sequentially to obtain each image's global transform.

We adopt regular step gradient descent optimizer [9] in the *interpolator* and *optimizer* stages. We model the *transform* using rigid 2D transform, which allows 2D rotation and translation. This choice is based on the physical conditions that the tissue does not elastically deform during sectioning or mounting, that the microtome produces parallel sections, and that all images are acquired at the same magnification. The only variable components of the transform are in-plane rotation and translation.

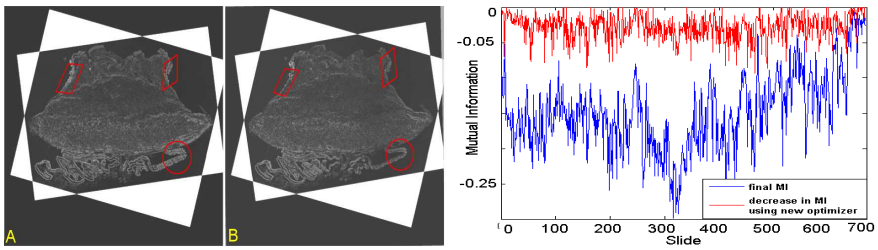

Fig. 5. Application of the regular step gradient descent (A) and the two-level optimizer (B) on PCA-aligned slides. Note that the regular step gradient descent settles in local solutions. Right: Plot showing the metric values after convergence (blue). The improvement in metric values using the two-level versus the standard optimizer is also shown (red). Note that the negative of mutual information is plotted.

We apply the multiresolution approach, using 2-level image pyramids as shown in Fig. 3 (Right). Optimal transforms obtained from a lower magnification (X_n) are scaled and used as initialization for registration of the next higher magnification (X_{n+1}). The process is repeated for each magnification level to obtain the final transforms. We note that at magnifications higher than *20x*, the computational cost for registration outweighs the improvements in accuracy.

4 Two-level Optimization

Tissue detection and PCA-based image alignment significantly improved registration performance by reducing the search space for the optimal transform. However, 3D visualization of the registered placenta revealed that the transforms remained suboptimal. Experiments with different optimizers such as conjugate-gradient and gradient descent did not affect performance significantly due to overtly noisy metrics. We propose the use of a novel two-level optimization scheme by searching the transform space neighborhood with a random walk strategy.

Optimizers such as regular-step gradient descent and conjugate gradient ([9]) increase the rate of convergence by refining the transform based on their current learning rates from observed MI gradients. However, their performance degrades rapidly since the learning rates are sensitive to data noise. In the placenta data, we observe that ITK optimizers converge to local solutions as shown in Fig. 5(A) for most image pairs (better MI values were later observed with the two-level optimizer).

We use a two-level optimization strategy, which perturbs converged solutions via random walks and then restarts the normal registration process. In essence, the perturbation introduces a step in the transform space that is larger than the specified learning rate of the regular step gradient descent optimizer. The step is a restricted translation and rotation around the PCA initialization. If the previous result was a local minimum, then the perturbation may result in a better

solution with higher MI (lower -MI) as shown in Fig. 5 (B) and a new solution is realized. The process is repeated until the MI does not improve even after an user-defined N perturbations. Similar to standard optimizers, convergence to a global solution is not guaranteed. However, the registration is likely to perform better since this approach allows hill climb against the gradient direction.

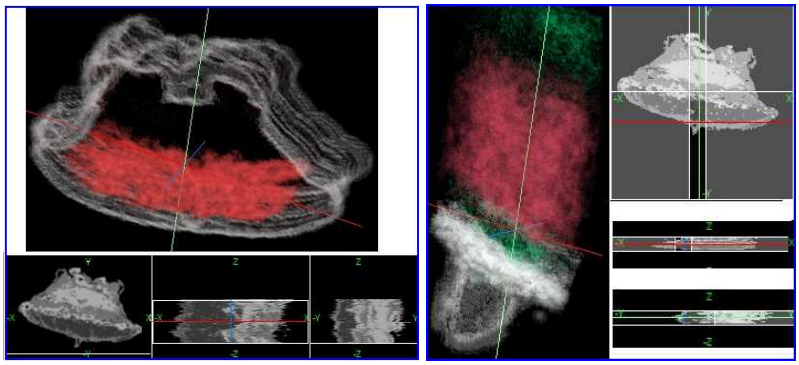

Fig. 6. Left: 3D visualization of the labyrinth layer within the placenta slices, shown as white boundaries. Right: A single finger like infiltration from the spongiotrophoblast into the labyrinth is zoomed and shown.

In the placenta images, we determined that maximum transform deviation of PCA aligned images is ± 80 pixels in translation and ± 10 degrees in rotation around the tissue centroid. The hybrid optimization strategy lead to global solutions in 99% of the images within N=20 iterations. The remaining 1% converges within N=50 iterations. Figure 5 (Right) shows the plots of the final MI values of all the images (blue) using the two-level optimizer. The improvement of the two-level optimizer compared to standard optimizer is shown as a difference in the MI values at convergence (red). The average negative MI of all images using the standard and two-level optimizers are -0.122 and -0.142 respectively. Figure 6 (Left) shows the 3D visualization of the labyrinth layer and the placenta contours. Figure 6 (Right) show the zoomed cross-section of a single finger like infiltration from the spongiotrophoblast into the labyrinth layer. Figure 7 is yet another example of finger visualization.

5 Conclusion and Future Work

In this paper, we described our experience in registering large serial sections of a histology sample. Our contribution involves methods to adapt the ITK registration process for real-world data such as the mouse placenta. We utilized pre-processing techniques to account for acquisition artifacts, defective histology sections, and large parameter search space. We also employed a multi-resolution implementation of MI registration algorithm. We propose a new optimization

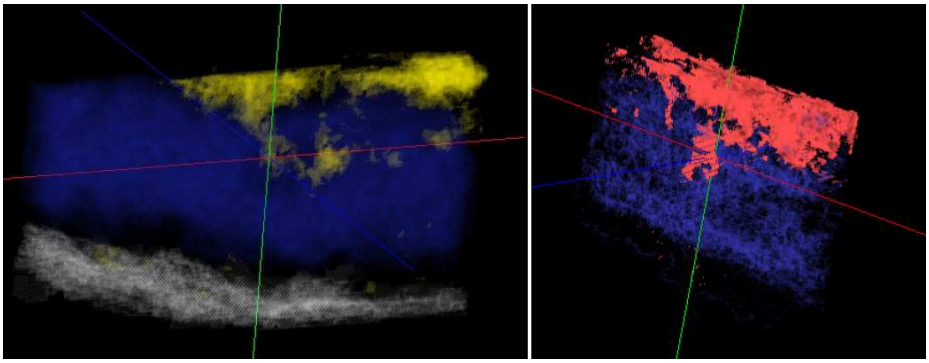

Fig. 7. Both images are cropped volumes from the original dataset focusing on infiltrations into the labyrinth layer. In both images the labyrinth is shown in blue. In the top image glycogen is shown in yellow and placenta boundary in white, while the bottom image highlights glycogen in red. The cross-hairs indicate the center of the infiltration into the labyrinth layer.

strategy that has a higher probability of convergence to global solutions albeit with longer processing times. Our results show an improvement in the final 3D reconstructions and overall lower MI metric values.

References

1. Mouse Genome Sequencing Consortium: Initial sequencing and comparative analysis of the mouse genome. Nature **420** (2002) 520–562
2. Wu, L., de Bruin, A., Saavedra, H.I., Starovic, M., Trimboli, A., Yang, Y., Opavska, J., Wilson, P., Thompson, J.C., Ostrowski, M.C., Rosol, T.J., Woollett, L.A., Weinstein, M., Cross, J.C., Robinson, M.L., Leone, G.: Extra-embryonic function of Rb is essential for embryonic development and viability. Nature **421** (2003) 942–947
3. Ibáñez, L., Schroeder, W.: The ITK Software Guide. The Insight and Registration Toolkit [www.itk.org], Kitware, Inc. (2003)
4. Rao, K., Machiraju, R., Heverhagen, J., Saltz, J., Knopp, M.: Exploratory segmentation using geometric tessellations (in presss). In: Proceedings of 10th International Fall Workshop on Vision, Modeling and Visualization. (2005)
5. Malladi, R., Sethian, J.A., Vermuri, B.C.: Shape modeling with front propagation: A level set approach. IEEE Trans. on Pattern Analysis and Machine Intelligence **17(2)** (1995) 158–174
6. Maintz, J.A.B.: Retrospective registration of tomographic brain images. Ph.D. dissertation, Univ. Utrecht, Utrecht, The Netherlands (1996)
7. Maes, F., Vandermeulen, D., Suetens, P.: Medical image registration using mutual information. Proceedings of the IEEE **91(10)** (1996) 1699–1722
8. Maes, F., Collignon, A., Vandermeulen, D., Marchal, G., Suetens, P.: Multimodality image registration by maximization of mutual information. IEEE Trans. Medical Imaging **16(2)** (1997) 187–198
9. Maes, F., Vandermeulen, D., Suetens, P.: Comparative evaluation of multiresolution optimization strategies for multimodality image registration by maximization of mutual information. Medical Image Analysis **3(4)** (1999) 373–386